ANZIAM J. 54(2013), 200–215
doi:10.1017/S1446181113000199

INTEGRATED PID CONTROLLER DESIGN FOR AN UNMANNED AERIAL VEHICLE WITH STATIC STABILITY

R. LI[✉1], Y. J. SHI[2] and H. L. XU[3]

(Received 21 January, 2012; revised 28 November, 2012)

Abstract

This paper presents an integrated guidance and control (IGC) design method for an unmanned aerial vehicle with static stability which is described by a nonlinear six-degree-of-freedom (6-DOF) model. The model is linearized by using small disturbance linearization. The dynamic characteristics of pitching mode, rolling mode and Dutch rolling mode are obtained by analysing the linearized model. Furthermore, an IGC design procedure is also proposed in conjunction with a proportional–integral–derivative (PID) control method and fuzzy control method. A PID controller is applied in the control loop of the elevator and aileron, and the attitude angle and attitude angular velocity are used as compensation feedback, giving a simple and low-order control law. A fuzzy control method is applied to perform the cross-coupling control of rolling and yawing. Finally, the 6-DOF simulation shows the effectiveness of the developed method.

2010 *Mathematics subject classification*: primary 34H05; secondary 93C95, 93C42.

Keywords and phrases: unmanned aerial vehicle, integrated guidance and control, fuzzy control, short-term motion, static stability.

1. Introduction

In past decades, most flight control systems were designed by using the traditional separate design method, that is, the guidance and control systems were designed separately and then integrated into one system. If the overall system performance was not satisfactory, the whole system would be redesigned to improve performance. This design method is not truly optimal and the overall system performance tends to be overconservative. Thus, an efficient method, called the integrated guidance and control (IGC) system design methodology, was proposed by Yueh and Lin [15] to improve

[1]School of Automation, University of Electronic Science and Technology of China, Chengdu, China; e-mail: hitlirui@gmail.com.
[2]School of Aeronautics and Astronautics, University of Electronic Science and Technology of China, Chengdu, China; e-mail: shiyingjing@gmail.com.
[3]School of Information Science and Engineering, Central South University, Changsha, China; e-mail: H.Xu@curtin.edu.au.

the overall performance. The IGC design method also improves system safety and reliability by removing one loop.

Recently, the IGC design method has been extensively studied in the literature. A sliding-mode controller was derived for an integrated missile autopilot and guidance loop by Idan et al. [4, 11]. To evaluate the performance of the various guidance and control solutions, a two-dimensional nonlinear simulation of the missile lateral dynamics and relative kinematics was used [11] and the additional degree of freedom (DOF) was then used [4] to account for the guidance and autopilot requirements. However, the linearized models of Idan et al. [4, 11] are all formulated under the limitation that the angle between line of sight and missile velocity is small or almost constant. Backstepping control was used to design IGC laws with a higher-order sliding-mode observer by Hwang and Tahk [3]. The stability of the integrated backstepping guidance and control logic was proven using the Lyapunov method. However, the approaches of Hwang and Tahk [3] may not strictly maintain the stability of the overall system. The feedback linearization technique was employed by Menon et al. [7] for the IGC of a moving-mass actuated kinetic warhead, and a 9-DOF simulation model of a kinetic warhead was developed with three moving-mass actuators. However, the feedback linearization could result in a large control and it is only applicable to systems which satisfy some conditions of feedback linearizability. A prototype fully integrated missile guidance and control system has been discussed by Palumbo and Jackson [8]. The IGC problem was formulated as a single nonlinear minimax optimization problem, which was handled by the state-dependent Riccati technique. However, as mentioned in that paper, solving the state-dependent Riccati equation online was time consuming. Particularly for a 6-DOF missile with an IGC design, the system order would grow much higher. Many other IGC schemes have been developed to incorporate various control theories [2, 5, 6, 9, 12, 14].

Most of these IGC methods are designed for missiles. Furthermore, most of these existing design results are theoretical, and are difficult to use in engineering. In this paper we apply the IGC design method to an unmanned aerial vehicle which is derived from a real airplane model. The main contribution of this paper is twofold. First, it provides an IGC design method for an unmanned aerial vehicle. The aircraft studied has good static stability, which results in small control augmentation press; thus the inner loop and outer loop can be integrated. However, there exists strong lateral-directional coupling, and hence a fuzzy controller is introduced to achieve cross control of rolling and yawing. Therefore, an IGC method using a proportional–integral–derivative (PID) controller and fuzzy controller is introduced in this paper. Second, the IGC method is applied to an unmanned aerial vehicle with low flight velocity and low cost, making it suitable for use in geological exploration and frontier inspection.

The rest of the paper is organized as follows. The common design method for aircraft, where the control and guidance loop are designed separately, is described in Section 2. Then the structure of the IGC design method is introduced. The linearized model of the unmanned aerial vehicle is presented in Section 3. Analysis of the airplane ontology shows that the IGC design can be applied for this unmanned aerial

https://doi.org/10.1017/S1446181113000199 Published online by Cambridge University Press

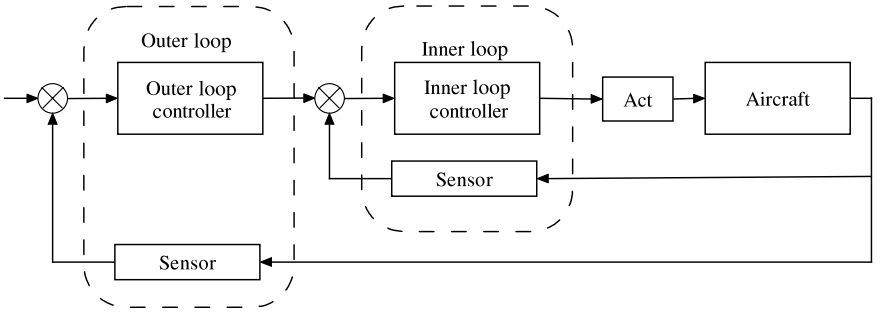

FIGURE 1. Logic diagram of control and guidance loops designed separately.

vehicle to achieve better control efficiency. Furthermore, the IGC design method is concretely proposed for the aircraft. The nonlinear 6-DOF simulation results are given in Section 4 to demonstrate the potential applications of the proposed IGC approach.

2. Structure and advantages of the IGC design

The design structure where the control and guidance loops are designed separately is depicted in Figure 1. The control loop is the inner loop, which aims to achieve control augmentation. A sensor is used in the inner loop to feed back information on the attitude angle and attitude angular velocity. For some high speed and large envelope airplanes, information on the attack angle and sideslip angle is also needed. The guidance loop is the outer loop, which aims to maintain the flight path and flight attitude. A sensor is used in the outer loop to feed back position and attitude angle information.

The integrated design structure is shown in Figure 2, where guidance and control loops are merged into one loop. A sensor is used to feed back the position, attitude angle and attitude angular velocity of the airplane, where position information is used to realize flight path and attitude angle information is used to achieve control augmentation. It should, however, be pointed out that the applicability of this design method depends on the ontology performance of the airplane. If the integrated design method is used to design a system which includes the feedback loop in the inner and outer loop, then the order of the control law is significantly decreased.

Suppose that the guidance and control loops are designed separately. Then a PID control method can be used for both the inner and outer loops, where the inner loop control law is

$$G_I^c(s) = K_I^p\left(1 + \frac{1}{T_I^i s} + T_I^d s\right).$$

Here K_I^p denotes the controller gain; T_I^i and T_I^d denote the time constants of the integral term and differential term, respectively; the subscript I denotes the inner loop; the superscript c denotes the control law; and the superscripts p, i and d denote,

https://doi.org/10.1017/S1446181113000199 Published online by Cambridge University Press

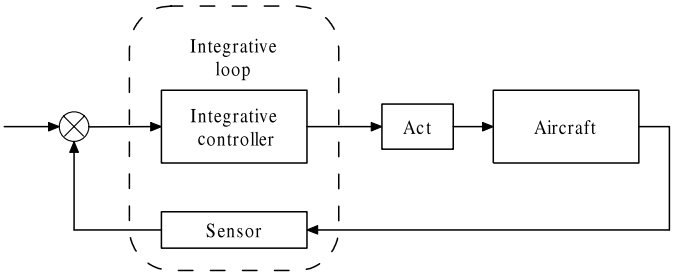

FIGURE 2. Structure diagram of integrated design of guidance and control loops.

respectively, the proportional, integral and differential terms. Denote the transfer function of the airplane ontology by $G(s)$. By using the Mason formula, we obtain the closed loop transfer function of the inner loop,

$$G_{IC}(s) = \frac{G_I^c(s) \times G(s)}{1 + G_I^c(s) \times G(s)},$$

where the subscript C denotes the closed loop. The control law of the outer loop is

$$G_O^c(s) = K_O^p\left(1 + \frac{1}{T_O^i s} + T_O^d s\right),$$

where K_O^p denotes the controller gain, T_O^i and T_O^d denote the time constants of the integral and differential terms, respectively, and the subscript O denotes the outer loop. Similarly, by using the Mason formula, we obtain the transfer function of the whole loop,

$$G_{OC}(s) = \frac{G_O^c(s) \times G_I^c(s) \times G(s)}{1 + G_I^c(s) \times G(s) + G_O^c(s) \times G_I^c(s) \times G(s)}, \tag{2.1}$$

where the subscript and superscript notation is as above.

Suppose that a PID control method is used for the IGC design. Then the integrated control law is

$$G^c(s) = K^p\left(1 + \frac{1}{T^i s} + T^d s\right),$$

where, similarly, K^p denotes the controller gain, T^i and T^d denote the time constants of the integral and differential terms, respectively, and the superscript c again denotes the control law. The overall closed-loop transfer function is

$$G_C(s) = \frac{G^c(s) \times G(s)}{1 + G^c(s) \times G(s)}. \tag{2.2}$$

Comparison of (2.1) with (2.2) shows that when the guidance and control loops are designed separately, the order N_{sep} of the closed loop system satisfies

$$N_{\text{sep}} = 2 + 2 + N,$$

https://doi.org/10.1017/S1446181113000199 Published online by Cambridge University Press

where N denotes the order of the transfer function of the outer airplane ontology. When the IGC design is used, the order N_{int} of the closed-loop system satisfies

$$N_{\text{int}} = 2 + N.$$

The order of the closed-loop system is lower when the IGC design is used.

The element error and other unpredictable errors would also be reduced by removing one loop. Furthermore, when the airborne code is compiled, the probability of logic error and code realization error would be reduced. Consequently, the safety and reliability of the system are improved.

3. IGC design

3.1. Analysis of airplane ontology From classical mechanics, we obtain the following centroid kinetic equations of the airplane:

$$\begin{aligned} m\left(\frac{du}{dt} + qw - rv\right) &= T\cos\varphi - D\cos\alpha\cos\beta - Y\cos\alpha\sin\beta \\ &\quad + L\sin\alpha - mg\sin\theta, \\ m\left(\frac{dv}{dt} + ru - pw\right) &= -D\sin\beta + Y\cos\beta + mg\sin\phi\cos\theta, \\ m\left(\frac{dw}{dt} + pv - qu\right) &= -T\sin\varphi - D\sin\alpha\cos\beta - Y\sin\alpha\sin\beta \\ &\quad - L\cos\alpha + mg\cos\phi\cos\theta. \end{aligned} \tag{3.1}$$

Here m is the mass of the airplane; u, v, w are the velocity components of the mass centre motion in the geographic coordinates; p, q, r are the angular velocity components around the centroid in the body axis system; T is the engine thrust; φ is the engine installation angle; α, β are the attack angle and sideslip angle, respectively; g is gravitational acceleration; and θ, ϕ are the pitching angle and rolling angle, respectively. The kinetic equations of the airplane around the centroid are

$$\begin{aligned} I_x\frac{dp}{dt} + (I_z - I_y)qr - I_{zx}\left(pq + \frac{dr}{dt}\right) &= R, \\ I_y\frac{dq}{dt} + (I_x - I_z)rp + I_{zx}(p^2 + r^2) &= M, \\ I_z\frac{dr}{dt} + (I_y - I_x)pq + I_{zx}\left(qr - \frac{dp}{dt}\right) &= N, \end{aligned}$$

where I_* is the corresponding component of the inertial tensor and R, M, N are the rolling moment, pitching moment and yawing moment, respectively. The centroid

https://doi.org/10.1017/S1446181113000199 Published online by Cambridge University Press

kinematic equations of the airplane are

$$\begin{aligned}\frac{dx_g}{dt} &= u\cos\theta\cos\psi + v(\sin\theta\sin\phi\cos\psi - \cos\phi\sin\psi)\\ &\quad + w(\sin\theta\cos\phi\cos\psi + \sin\phi\sin\psi),\\ \frac{dy_g}{dt} &= u\cos\theta\sin\psi + v(\sin\theta\sin\phi\sin\psi + \cos\phi\cos\psi)\\ &\quad + w(\sin\theta\cos\phi\sin\psi - \sin\phi\cos\psi),\\ \frac{dz_g}{dt} &= -u\sin\theta + v\sin\phi\cos\theta + w\cos\phi\sin\theta,\end{aligned}$$

where x_g, y_g, z_g are the centroid coordinate components of the airplane in the geographic coordinates and ψ is the yaw angle. The kinematic equations of the airplane around the centroid are

$$\begin{aligned}\frac{d\phi}{dt} &= p + \tan\theta(q\sin\phi + r\cos\phi),\\ \frac{d\theta}{dt} &= q\cos\phi - r\sin\phi,\\ \frac{d\psi}{dt} &= \frac{1}{\cos\theta}(q\sin\phi + r\cos\phi).\end{aligned}$$

The 12 differential equations above are nonlinear and contain variable coefficients. It is difficult to solve them analytically. Thus, the linearization method is employed. In order to analyse the stability and maneuverability of the airplane, the characteristic points are chosen, at which the system is trimmed and linearized according to some specific flight modes (such as horizontal flying and steady circling). Here we apply the commands *findop* and *linearize* in Matlab to achieve the trimming and linearization. By trimming and linearizing the 6-DOF nonlinear ontology model, we obtain the longitudinal equations of the unmanned aerial vehicle as follows:

$$\dot{\mathbf{x}} = \begin{bmatrix} -0.611 & -0.039 & 0.005 & 0\\ 50.8 & -1.728 & -0.412 & -0.684\\ -3.553 & 0.176 & -0.036 & -9.779\\ 1 & 0 & 0 & 0\end{bmatrix}\mathbf{x} + \begin{bmatrix} -3.408\\ -5.569\\ 0.023\\ 0\end{bmatrix}\mathbf{u}, \tag{3.2}$$

where $\mathbf{x} = [\Delta Q \quad \Delta W \quad \Delta U \quad \Delta\theta]^{\mathrm{T}}$; $\mathbf{u} = \Delta\delta_e$; ΔQ is the increment of the pitching angular velocity; ΔW is the increment of the z axial velocity component with the body axes coordinate system; ΔU is the increment of the x axial velocity component with the body axes coordinate system; $\Delta\theta$ is the pitching angle increment; and $\Delta\delta_e$ is the increment of the elevator deflection angle. By solving the characteristic function of (3.2), it follows that the damping ratio of the pitching mode is 0.673 and the undamped oscillation frequency is 1.76 rad s^{-1}. The linearized lateral-directional

https://doi.org/10.1017/S1446181113000199 Published online by Cambridge University Press

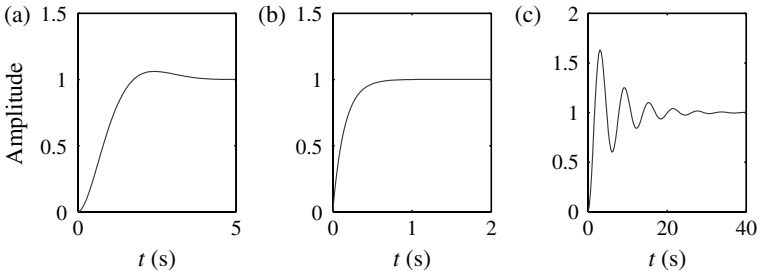

FIGURE 3. Step response of (a) pitching mode, (b) rolling mode and (c) Dutch rolling mode.

equations of the unmanned aerial vehicle are

$$\dot{\mathbf{x}} = \begin{bmatrix} -0.116 & 3.553 & -50.8 & 9.779 \\ -0.064 & -6.775 & 0.048 & 0 \\ 0.019 & 0.017 & -0.163 & 0 \\ 0 & 1 & 0.07 & 0.011 \end{bmatrix} \mathbf{x} + \begin{bmatrix} 0.111 & 6.375 \\ -10.64 & 4.656 \\ 0.012 & -2.981 \\ 0 & 0 \end{bmatrix} \mathbf{u}, \tag{3.3}$$

where $\mathbf{x} = [\Delta V \quad \Delta P \quad \Delta R \quad \Delta\phi]^{\mathrm{T}}$; $\mathbf{u} = [\Delta\delta_a \quad \Delta\delta_r]^{\mathrm{T}}$; ΔV is the increment of the y axial velocity component with the body axes coordinate system; ΔP is the increment of the rolling angular velocity; ΔR is the increment of the yawing angular velocity; $\Delta\phi$ is the increment of the rolling angle; $\Delta\delta_a$ is the increment of the aileron deflection angle; and $\Delta\delta_r$ is the increment of the rudder deflection angle. By solving the characteristic function of (3.3), it follows that the damping ratio of the rolling mode is 1, and the undamped oscillation frequency is 6.75 rad s^{-1}. The damping ratio of the Dutch rolling mode is 0.15, and the undamped oscillation frequency is 1.04 rad s^{-1}.

Figures 3(a–c) show the step response curves of the pitching mode, lateral-directional rolling mode and Dutch rolling mode, respectively. We see that the stability of the pitching mode and the rolling mode is good, while the damping ratio of the Dutch rolling mode is small, but the oscillation period is long. Since the number of oscillations of the pitching mode and lateral-directional rolling mode is less than 3, the first flying quality requirement described by Zhang [16] is ensured, namely that the aircraft can perform all given flight tasks. For the Dutch rolling mode, we see from Figure 3 that the oscillation occurs several times; however, the oscillation period is long (over 15 seconds), which is accepted by the flying qualities requirement [16]. Thus, the aircraft studied has good static stability. Therefore, the IGC design can be applied for this unmanned aerial vehicle to achieve better control efficiency.

3.2. Design of the PID control law for the elevator and aileron Although wide choices for control schemes are offered with advanced developments in digital technology, more than 90% of industrial controllers are still implemented based around PID algorithms, since no other controllers can match the simplicity, clear functionality, applicability, and ease of use offered by the PID controller [1]. Therefore, in this paper

https://doi.org/10.1017/S1446181113000199 Published online by Cambridge University Press

Table 1. Design parameters of the elevator control law.

θ_c	K_e^{Hp}	K_e^{Hi}	K_e^{Hd}	$K_e^{\theta p}$	$K_e^{\theta d}$
0.3	0.3	0.1	0.5	1.5	1.0

Table 2. Design parameters of aileron control law.

K_ψ^ϕ	$K_a^{\phi p}$	$K_a^{\phi i}$	$K_a^{\phi d}$
1.0	1.5	0.5	0.5

the PID control method is applied for controller design of the main channels of the elevator and aileron.

When the IGC method is applied, the altitude feedback is the guidance loop, and the pitching angle feedback and pitching angular velocity feedback are the control loop to achieve compensation. The control law of the elevator is designed as follows:

$$\delta_e = K_e^{Hp}(H - H_c) + K_e^{Hi}\int (H - H_c)\,dt + K_e^{Hd}\frac{d(H - H_c)}{dt} + K_e^{\theta p}(\theta - \theta_c) + K_e^{\theta d}Q,$$

where H is the flight height of the airplane; H_c is the instruction flight height; θ is the current pitching angle; θ_c is the trim pitching angle; Q is the current pitching angular velocity; and K_e^{Hp}, K_e^{Hi}, K_e^{Hd}, $K_e^{\theta p}$, $K_e^{\theta d}$ are the design parameters of the elevator control law. The trim pitching angle is determined by the flight state and is set as 0.3.

The bank to turn (BTT) method is used for the track path angle in the lateral-directional control. The control law of the aileron is

$$\delta_a = K_a^{\phi p}(\phi - \phi_c) + K_a^{\phi i}\int (\phi - \phi_c)\,dt + K_a^{\phi d}P,$$

where ϕ is the current rolling angle; ϕ_c is the instruction rolling angle; P is the current rolling angular velocity; and $K_a^{\phi p}$, $K_a^{\phi i}$, $K_a^{\phi d}$ are the design parameters of the aileron control law. The instruction rolling angle satisfies

$$\phi_c = K_\psi^\phi(\psi - \psi_c),$$

where ψ is the current yaw angle, ψ_c is the instruction yaw angle and K_ψ^ϕ is the design parameter of the aileron control law. The design parameters of the elevator and aileron control laws can be obtained by the parameterized method given by Shi and Li [10]. They are listed in Tables 1 and 2.

3.3. Fuzzy controller design for the rudder For the rudder, cross-coupling control of the aileron and rudder is applied, that is,

$$\Delta\delta_r = K_{\text{ari}}\Delta\delta_a. \tag{3.4}$$

https://doi.org/10.1017/S1446181113000199 Published online by Cambridge University Press

In the following, we show how to solve for the cross-coupling gain K_{ari}. Equation (3.1) can be written as:

$$\begin{aligned} m\left(\frac{du}{dt} + qw - rv\right) &= F_x, \\ m\left(\frac{dv}{dt} + ru - pw\right) &= F_y, \\ m\left(\frac{dw}{dt} + pv - qu\right) &= F_z. \end{aligned} \tag{3.5}$$

In addition, it is known that

$$u = V\cos\alpha\cos\beta, \quad v = V\sin\beta, \quad w = V\sin\alpha\cos\beta.$$

When the sideslip angle β is small, the foregoing formulation can be approximated as:

$$u = V\cos\alpha, \quad v = V\beta, \quad w = V\sin\alpha.$$

When the short-term motion is considered, V is usually assumed constant. Then, substituting the above formulation into the second equation of (3.5), we obtain

$$m\left(V\frac{d\beta}{dt} + rV\cos\alpha - pV\sin\alpha\right) = F_y. \tag{3.6}$$

From the flight dynamics, we can assume that, when the sideslip angle β is small, the side force in (3.6) satisfies $F_y = 0$. Thus, for keeping $\dot{\beta} \to 0$,

$$\frac{r}{p} = \tan\alpha. \tag{3.7}$$

Here r is the yaw rate and p is the roll angular velocity. These are functions of the aileron and rudder deflection angle. Expanding (3.7),

$$\frac{N_{\delta_a}\Delta\delta_a + N_{\delta_r}\Delta\delta_r}{R_{\delta_a}\Delta\delta_a + R_{\delta_r}\Delta\delta_r} = \tan\alpha.$$

Considering the cross-coupling control law (3.4),

$$\frac{N_{\delta_a}\Delta\delta_a + N_{\delta_r}K_{\text{ari}}\Delta\delta_a}{R_{\delta_a}\Delta\delta_a + R_{\delta_r}K_{\text{ari}}\Delta\delta_a} = \tan\alpha.$$

Then the cross-coupling gain K_{ari} can be obtained as follows:

$$K_{\text{ari}} = -\frac{N_{\delta_a} - R_{\delta_a}\tan\alpha}{N_{\delta_r} - R_{\delta_r}\tan\alpha}.$$

The cross-coupling gain K_{ari} is relative to the angle of attack. Therefore, it must be adjusted with reference to the angle of attack.

https://doi.org/10.1017/S1446181113000199 Published online by Cambridge University Press

Table 3. Membership functions for the fuzzy controller.

Variable	γ		θ		δ_r	
	Type	Parameter	Type	Parameter	Type	Parameter
NB	Trapezoid	[−Inf−Inf − 15 − 6]	Trapezoid	[−Inf−Inf − 20 − 11]	Trapezoid	[−Inf−Inf − 0.6 − 0.4]
NM	Triangle	[−18 − 10.5 − 3]	Triangle	[−25.5 − 16.5 − 5.5]	Triangle	[−0.6 − 0.4 − 0.1]
NS	Triangle	[−12 − 5.25 0]	Triangle	[−20 − 8.5 0]	Triangle	[−0.4 − 0.1 0.2]
NO	Triangle	[−6 0 1.5]	—	—	—	—
ZO	—	—	Triangle	[8.5 0 8.5]	Triangle	[−0.1 0 0.5]
PO	Triangle	[−1.5 0 6]	—	—	—	—
PS	Triangle	[0. 5.25 12]	Triangle	[0 8.5 20]	Triangle	[0 0.5 1]
PM	Triangle	[3 10.5 18]	Triangle	[5.5 16.5 25.5]	Triangle	[0.5 1 2]
PB	Trapezoid	[6 15 Inf Inf]	Trapezoid	[11 20 Inf Inf]	Trapezoid	[1 2 Inf Inf]

Table 4. Rules for the fuzzy controller.

θ	γ							
	NB	NM	NS	NO	PO	PS	PM	PB
NB	NB	NB	NB	NB	NB	NB	NB	NB
NM	NS	NS	NB	NB	NB	NB	NB	NB
NS	PS	PS	NM	NB	NB	NB	NB	NB
ZO	PB	PS	NS	NM	NM	NM	NM	NB
PS	PB	PM	PS	NS	NS	NS	NM	NM
PM	PB	PB	PM	PS	ZO	ZO	ZO	NS
PB	PB	PB	PB	PB	PM	PS	ZO	ZO

Since there is no sensor for the angle of attack in such low-cost airplanes, usually the angle of attack is replaced by the flight path angle γ and the attitude angle θ. Thus, a fuzzy controller is applied to the control law of the rudder due to good adaptability, where the inputs are the flight path angle γ and the attitude angle θ; the output is the cross-coupling gain of the aileron and the rudder; and the domains are $\gamma \in [-15, 15]$, $\theta \in [-20, 20]$ and $K_{\text{ari}} \in [-0.5, 2]$, respectively. The linguistic terms and membership functions are described by Table 3. In each membership function, N denotes negative; P denotes positive; ZO and O denote zero; and B, M and S denote big, middle and small, respectively. The membership functions of the flight path angle γ include NO and PO, aiming to improve the steady state precision [13]. The fuzzy controller rules are described in Table 4.

The output surface of the fuzzy control law is shown in Figure 4. When the airborne code is generated, the interpolation table is produced according to the output surface, and thus the real time response and the reliability of the flight control system are ensured.

https://doi.org/10.1017/S1446181113000199 Published online by Cambridge University Press

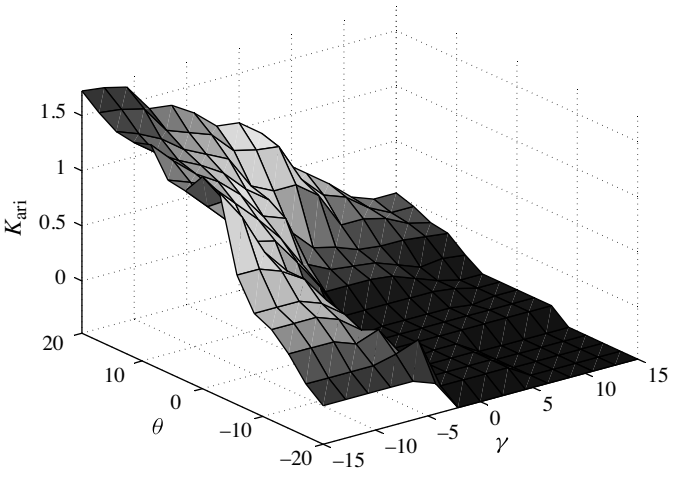

FIGURE 4. Output surface for the fuzzy controller.

4. Simulation and verification

In this section, the flight path control of an unmanned aerial vehicle is accomplished by the proposed method. The starting flight state is in the north horizontal direction and an altitude of 215 m. The task of lateral-directional flight is to maintain the flight path deflection angle. The longitudinal flight task is to track the instruction altitude, which is 215 m before 100 s and 315 m after 100 s. A fixed step size is used during the simulation course, which is 5 ms, and the simulation time is 800 s.

The simulation curves of the aileron, elevator and rudder deflection angles of the airplane are shown in Figures 5(a–c). Figure 5 shows that there is a slight aileron deflection during the flight course due to the lateral-directional asymmetry; the elevator helps the airplane to climb to the tracking altitude at 100 s; the rudder oscillates slightly as a result of the dead zone nonlinear elements, such as the rudder clearance. Fortunately, the oscillation amplitude is small and the oscillation period is long, which does not affect the flight.

The simulation curves of the rolling, pitching and yaw attitude angles are shown in Figure 6(a–c). Figure 6 shows that the rolling angle and the yaw angle can be well retained since the control law aims to accomplish the flight path tracking in the horizontal direction and the instruction flight path does not change, and the pitching angle responds to the instruction of the elevator to produce the corresponding increment, achieving altitude track.

The simulation curves of the rolling, pitching and yaw attitude angular velocities are shown in Figure 7(a–c). Figure 7 shows that the airplane has good stability performance.

The position and velocity simulation curves of the centroid motion are shown in Figure 8. Figure 8(a) shows how the altitude changes with time, where the ordinate is

https://doi.org/10.1017/S1446181113000199 Published online by Cambridge University Press

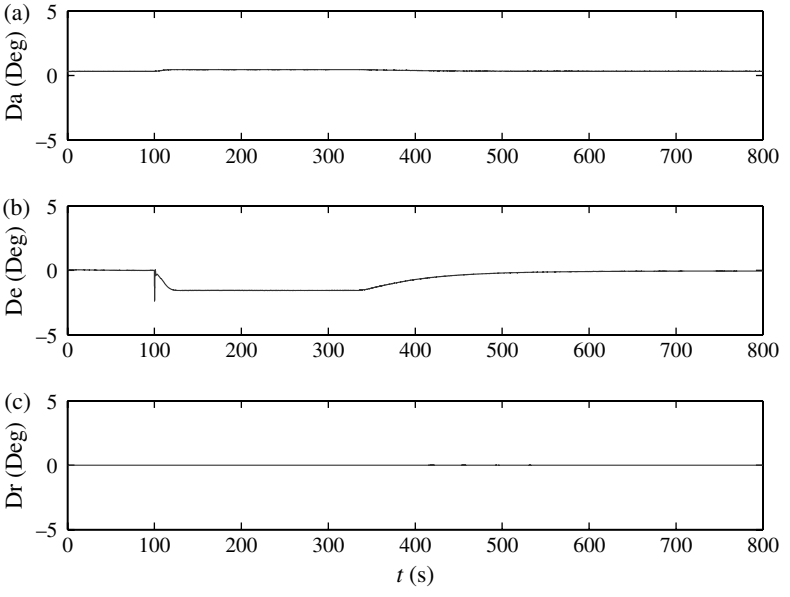

FIGURE 5. Deflection angle of (a) aileron, (b) elevator and (c) rudder.

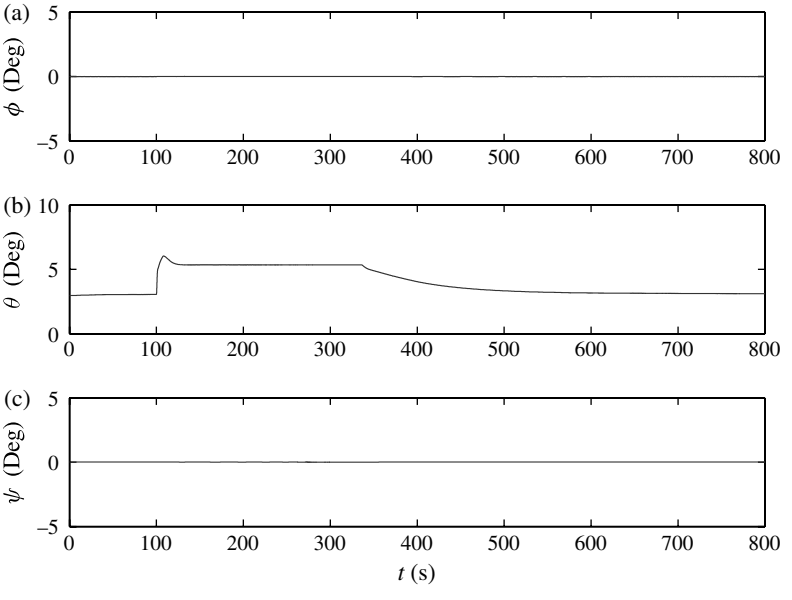

FIGURE 6. Simulation curve of the attitude angle: (a) rolling, (b) pitching, (c) yaw.

https://doi.org/10.1017/S1446181113000199 Published online by Cambridge University Press

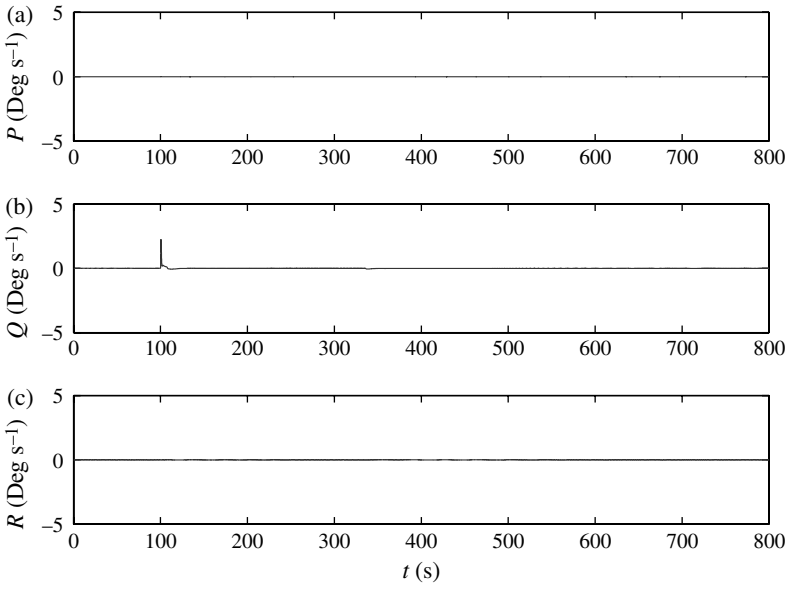

FIGURE 7. Simulation curve of the attitude angular velocity: (a) rolling, (b) pitching, (c) yaw.

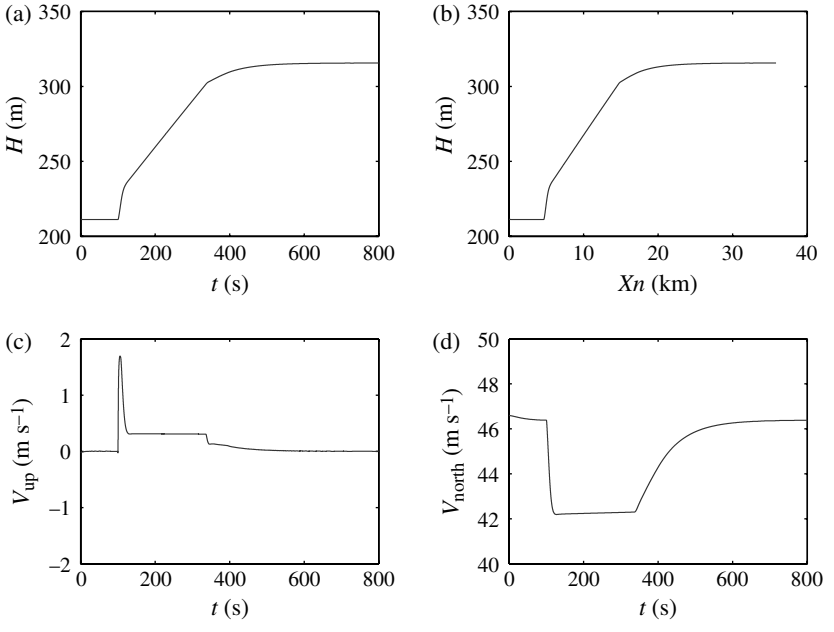

FIGURE 8. Position and velocity simulation curve of the centroid motion: (a) altitude, (b) altitude with abscissa the north flight distance, (c) climbing velocity, (d) north flight velocity.

https://doi.org/10.1017/S1446181113000199 Published online by Cambridge University Press

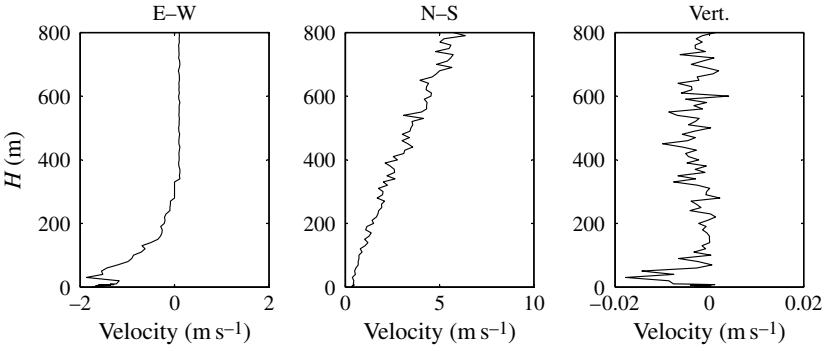

FIGURE 9. Schematic curve of real local wind: (a) east to west, (b) north to south, (c) downward.

the altitude of the airplane. During the simulation, the altitude of the airport is 15 m, that is, the airplane starts to fly at an altitude of 200 m relative to the airport at 100 s, and after 500 s it climbs to a relative altitude of 300 m and stays at this flight level. Figure 8(b) is also the simulation curve of the flight altitude, while the abscissa is the north flight distance. Figure 8(c) is the simulation curve of the upward flight velocity, that is, the climbing velocity. Figure 8(d) is the simulation curve of the north flight velocity. Figure 8 shows that the airplane can track the instruction flight path well and thus the desired flight task can be achieved.

In order to test the robustness of the proposed control method, we introduce the real local wind field, which is shown in Figure 9, where the abscissa is the velocity of the wind and the ordinate is the flying altitude. Figure 9(a) shows the component of wind from east to west; Figure 9(b) shows the component of wind from north to south; and Figure 9(c) shows the component of downward wind. The flight simulation curve with wind field test is shown as the solid lines in Figure 10, and the simulation curve without wind is shown as dotted lines in the same figure for comparison. The simulation curve of the pitching angle is shown in Figure 10(a). Since the aircraft flies against the wind, it is seen that the climbing time has increased. Figure 10(b) depicts the velocity simulation curve of northward flight. It is seen from the figure that flight velocity is apparently affected by the wind. The simulation curve of the flight altitude is shown in Figure 10(c), which shows that the aircraft can perform the flight task well under the effect of wind.

5. Conclusions

The IGC design method for an unmanned aerial vehicle with low flight velocity and low cost was studied and a PID controller was designed to produce the elevator and aileron control law. For the coupling action of the rolling and yaw, a fuzzy control method was adapted to obtain the rudder control law. By using the IGC design, the structure of the control law is simplified, the order of the control law is decreased and the safety and reliability of the system are improved. The 6-DOF simulation results

https://doi.org/10.1017/S1446181113000199 Published online by Cambridge University Press

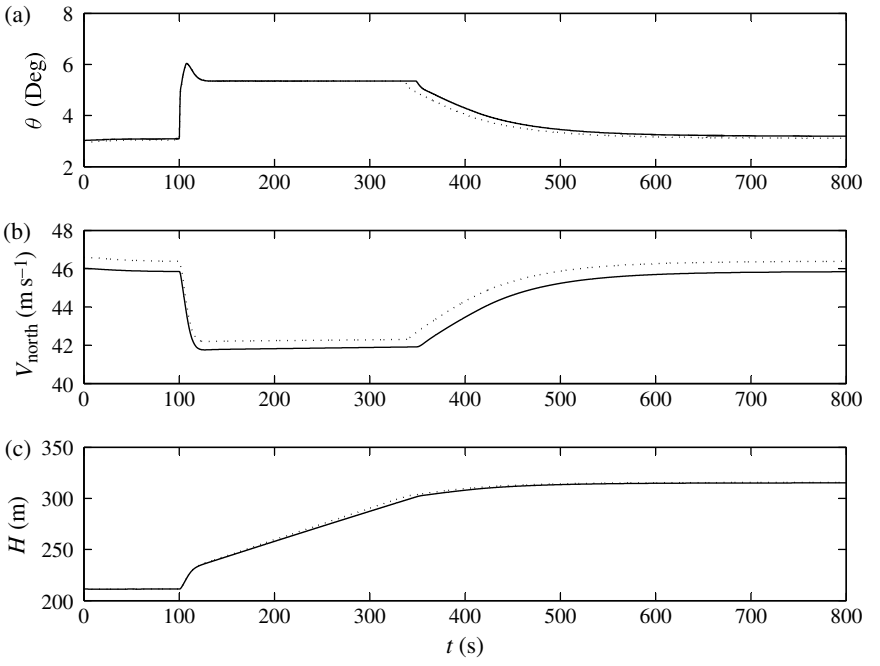

FIGURE 10. Flight simulation curve with wind: (a) pitching angle, (b) northward flight velocity, (c) altitude.

show that the designed control law can maintain good stability performance of the airplane and keep the track angle constant.

Acknowledgements

This work is supported by a grant from the 973 plan (No. 2011CB707005) and by the Fundamental Research Funds for the Central Universities (No. ZYGX2010J086).

References

[1] K. H. Ang, G. Chong and Y. Li, "PID control system analysis, design, and technology", *IEEE Trans. Contr. Syst. Tech.* **13** (2005) 559–576; doi:10.1109/TCST.2005.847331.

[2] G. R. Duan, M. Z. Hou and F. Tan, "Auxiliary system based integrated missile guidance and control", *2010 3rd International Symposium on Systems and Control in Aeronautics and Astronautics, Heilongjiang, China* 2010, 1276–1281; doi:10.1109/ISSCAA.2010.5633383.

[3] T. W. Hwang and M. J. Tahk, "Integrated backstepping design of missile guidance and control with robust disturbance observer", *SICE-ICASE International Joint Conference 2006, Busan, Korea*, 2006, 4911–4915; doi:10.1109/SICE.2006.314847.

[4] M. Idan, T. Shima and O. M. Golan, "Integrated sliding mode autopilot-guidance for dual-control missiles", *J. Guid. Contr. Dyn.* **30** (2007) 1081–1089; doi:10.2514/1.24953.

[5] P. K. Menon and E. J. Ohlmeyer, "Integrated design of agile missile guidance and control systems", *Proceedings of the 7th Mediterranean Conference on Control and Automation, Haifa, Israel*, 1999, 1469–1494; http://med.ee.nd.edu/MED7-1999/med99/papers/MED213.pdf.

[6] P. K. Menon and E. J. Ohlmeyer, "Nonlinear integrated guidance control laws for homing missiles", *AIAA Guidance, Navigation, and Control Conference, Montreal, Canada*, 2001.
[7] P. K. Menon, G. D. Sweriduk, E. J. Ohlmeyer and D. S. Malyevac, "Integrated guidance and control of moving-mass actuated kinetic warheads", *J. Guid. Contr. Dyn.* **27** (2004) 118–126; doi:10.2514/1.9336.
[8] N. F. Palumbo and T. D. Jackson, "Integrated missile guidance and control: a state dependent Riccati differential equation approach", *Proc. 1999 IEEE International Conference on Control Applications, Kohala Coast, USA*, 1999, 243–248; doi:10.1109/CCA.1999.806207.
[9] B. H. Sang and C. S. Jing, "Integrated guidance and control for a missile in the pitch plane based upon subspace stabilization", *2009 Chinese Control and Decision Conference, Guangxi, China*, 2009, 5409–5414; doi:10.1109/CCDC.2009.5195157.
[10] Y. J. Shi and R. Li, "Coordinated stability based trajectory tracking control law design of reconnaissance and attack UAV", *30th Chinese Control Conference, Yantai, China*, 2011, 3724–3729; http://ieeexplore.ieee.org/stamp/stamp.jsp?tp=&arnumber=6000709&isnumber=6000362.
[11] T. Shima, M. Idan and O. M. Golan, "Sliding-mode control for integrated missile autopilot guidance", *J. Guid. Contr. Dyn.* **29** (2006) 250–260; doi:10.2514/1.14951.
[12] I. Shkolnikov, Y. Shtessel and D. Lianos, "Integrated guidance-control system of a homing interceptor: sliding mode approach", *AIAA Guidance, Navigation, and Control Conference, Montreal, Canada*, 2001.
[13] T. Sreenuch, A. Tsourdos, E. J. Hughes and B. A. White, "Fuzzy gain-scheduled missile autopilot design using evolutionary algorithms", *American Control Conference, Portland, OR, USA*, 2005, 346–351; doi:10.1109/ACC.2005.1469957.
[14] M. Xin, S. N. Balakrishnan and E. J. Ohlmeyer, "Integrated guidance and control of missiles with Θ-D method", *IEEE Trans. Contr. Syst. Tech.* **14** (2006) 981–992; doi:10.1109/TCST.2006.876903.
[15] W. R. Yueh and C. F. Lin, "Optimal controller for homing missiles", *J. Guid. Contr. Dyn.* **8** (1985) 408–411; doi:10.2514/3.19997.
[16] M. L. Zhang, *Flight control systems* (Aviation Industry Press, Beijing, 1994).